



HAL
open science

On shear layer atomization within closed channels: Numerical simulations of a cough-replicating experiment

César Pairetti, Raphaël Villiers, Stéphane Zaleski

► To cite this version:

César Pairetti, Raphaël Villiers, Stéphane Zaleski. On shear layer atomization within closed channels: Numerical simulations of a cough-replicating experiment. *Computers and Fluids*, 2021, 231, pp.105125. 10.1016/j.compfluid.2021.105125 . hal-03653064

HAL Id: hal-03653064

<https://hal.sorbonne-universite.fr/hal-03653064>

Submitted on 28 Apr 2022

HAL is a multi-disciplinary open access archive for the deposit and dissemination of scientific research documents, whether they are published or not. The documents may come from teaching and research institutions in France or abroad, or from public or private research centers.

L'archive ouverte pluridisciplinaire **HAL**, est destinée au dépôt et à la diffusion de documents scientifiques de niveau recherche, publiés ou non, émanant des établissements d'enseignement et de recherche français ou étrangers, des laboratoires publics ou privés.

On shear layer atomization within closed channels: numerical simulations of a cough-replicating experiment

Cesar Pairetti^{a,b,c}, Raphaël Villiers^a, Stéphane Zaleski^{a,d}

^a*Sorbonne Université and CNRS, Institut Jean Le Rond d'Alembert, UMR 7190, Paris, France*

^b*Centro Internacional Mecánica Computacional (CONICET - UNL), Santa Fe, Argentina*

^c*Facultad de Ciencias Exactas, Ingeniería y Agrimensura (UNR), Rosario, Argentina*

^d*Institut Universitaire de France, IUF, Institut Jean Le Rond d'Alembert, UMR 7190, Paris, France*

Abstract

Aerosol generation during coughing and sneezing has gained major relevance due to the current COVID pandemic. The atomization involved in this process takes place in the complex context of the respiratory system and develops very rapidly. In order to get further insights on the early spray generation, we introduce a simplified model of physiological coughing or sneezing, in the form of a thin liquid layer subject to a rapid (30 m/s) air stream. The setup is simulated using the Volume-Of-Fluid method with octree mesh adaptation, the latter allowing grid sizes small enough to capture the Kolmogorov length scale. The results confirm the trend to an intermediate distribution between a Log-Normal and a Pareto distribution $P(d) \propto d^{-3.3}$ for the distribution of droplet sizes in agreement with a previous re-analysis of experimental results by one of the authors. The mechanism of atomization does not differ qualitatively from the multiphase mixing layer experiments and simulations. No mechanism for a bimodal distribution, also sometimes observed, is evidenced in these simulations.

1. Introduction

Coughing and sneezing are two processes by which a large number of droplets of muco-salivary fluid are exhaled and subsequently travel large distances in the environment [1, 2]. These phenomena have acquired an acute interest in the context of the so-called aerosol transmission route of the Covid-19 pandemic [3], but have been studied for near a century in the context of respiratory diseases in general [4]. Early investigations by Duguid [5] and Loudon & Roberts [6] of the number and size of droplets emitted in coughing and sneezing events have yielded rich data, incorporating very large numbers of droplets. More recently, Xie *et. al.* [7] proposed corrected droplet size distribution by estimating the in-flight evaporation process. In this context, a comprehensive analysis of the characteristics of these droplets, both in size and

Email address: stephane.zaleski@sorbonne-universite.fr (Stéphane Zaleski)

velocity, would be of immense interest, as it is a prerequisite for modeling the droplet cloud propagating further downstream from the mouth [8, 9].

Rapid photographic imaging [10] has revealed features similar to those observed in other *atomization* processes, including thin liquid sheets, ligaments and droplets. In this context, the statistical distribution of droplet sizes is of particular interest. Although the log-normal distribution has been frequently mentioned in connection with exhalations [11, 12] as for other atomizing flows [13] many other distributions $N(d)$ of the diameter d have been put forward such as compound gamma distributions [14] and many others. A re-analysis of the data of Duguid and Loudon & Roberts for sneezes has however revealed [3] a $N(d) \sim d^{-2}$ scaling over an impressive three orders of magnitude. This scaling allows determining the proportion of millimeter-sized droplets that travel short distances and the proportion of much smaller droplets that can be incorporated in a turbulent puff or particle-laden jet and travel long distances as discussed in ref. [1, 3]. The fraction of the exhaled muco-salivary fluid in each class of droplet sizes may also be determined in this way and the probability of having viral loads in each class can be inferred under adequate hypotheses, such as a homogeneous distribution of the virus in volume or surface.

In order to better understand the fluid mechanics of exhalations, King, Brock & Lundell [15] have designed a physical model of violent exhalation that may be nicknamed a “cough machine”. Air is flowing at high speed (from 10 to 30 m/s) in a rectangular-section duct, with a flow rate analog of the observed human cough. A thin layer of muco-salivary fluid is deposited at the bottom of the duct. While King, Brock & Lundell use the cough machine to observe non-atomizing waves on the thin layer, it can also be used to simulate droplet formation at higher speeds and/or lower velocities. The device would then achieve atomization through a process similar to that of shear flow atomization of planar sheets [16, 14, 17, 13, 18, 19]. (See also the recent review of numerical approaches in [20].) However there are important differences since the liquid layer is initially at rest and the airflow is impulsive. These differences could lead to different distributions of droplet sizes and velocities, which are the focus of the current investigation.

2. Numerical method and setup

We model both the muco-salivary fluid and the surrounding gas as incompressible Newtonian fluids. This hypothesis is valid considering that non-newtonian effects on the liquid are only relevant for very small scales. In a context of uniform temperature and high relative humidity, such as a human trachea or a long channel experiment, heat transfer and evaporation will be negligible. Moreover, during the short duration of the atomization process, heat and mass transfer will not have time to develop significantly. Thus the flow is described by the Navier-Stokes equations:

$$\nabla \cdot \vec{u} = 0 \tag{1}$$

$$\frac{\partial \rho \vec{u}}{\partial t} + \nabla \cdot (\rho \vec{u} \vec{u}) = -\nabla p + \nabla \cdot (2\mu \mathbf{D}) + \sigma \kappa \vec{n}_s \delta_s \tag{2}$$

where $\vec{u}(\vec{x}, t)$ is the velocity field and $p(\vec{x}, t)$ is the pressure field. Tensor \mathbf{D} is equal to $\frac{1}{2} [\nabla \vec{u} + (\nabla \vec{u})^T]$. ρ and μ are the flow density and viscosity respectively. The last term on the right-hand side on the Navier-Stokes Equation 2 represents the surface tension force, where the coefficient σ is considered constant. The force only acts at the free surface, hence the Dirac function δ_s , and also depends on the interface shape, particularly on its curvature κ and normal \vec{n}_s .

We solve this set of equations by a simple finite volume discretization in the one-fluid numerical approach for two-phase flow, using a Volume-Of-Fluid (VOF) [21]. The VOF function at a grid cell is $f = \int c dV$, where c indicates the presence of the liquid ($c(\vec{x}, t) = 1$) or gas ($c(\vec{x}, t) = 0$) phase. The fluid properties at the cell are defined by arithmetic averages:

$$\rho = f\rho_l + (1 - f)\rho_g \quad \mu = f\mu_l + (1 - f)\mu_g \quad (3)$$

The discrete equations for this model can then be expressed as in [22]:

$$\frac{f^{n+\frac{1}{2}} - f^{n-\frac{1}{2}}}{\Delta t} + \nabla \cdot (\vec{u}_n f_n) = c_c \nabla \cdot \vec{u}^n \quad (4)$$

$$\frac{\rho \vec{u}^* - \rho \vec{u}^n}{\Delta t} + \nabla \cdot (\rho^{n+\frac{1}{2}} \vec{u}^n \vec{u}^n) = \nabla \cdot [\mu^{n+\frac{1}{2}} (\mathbf{D}^n + \mathbf{D}^*)] + (\sigma \kappa \delta_s \vec{n}_s)^{n+\frac{1}{2}} \quad (5)$$

$$\nabla \cdot \left(\frac{\Delta t}{\rho^{n+\frac{1}{2}}} \nabla p^{n+\frac{1}{2}} \right) = \nabla \cdot \vec{u}^* \quad (6)$$

$$\vec{u}^{n+1} = \vec{u}^* - \frac{\Delta t}{\rho^{n+\frac{1}{2}}} \nabla p^{n+\frac{1}{2}} \quad (7)$$

where c_c is the contraction function used in the split volume fraction advection scheme from [23] that give consistency to the mass balance. The advective fluxes on Equation (5) are integrated explicitly based on a momentum-conserving Bell-Collella-Glaz scheme[24] and the viscous term is computed in a semi-implicit manner. The surface tension force term is based on a discrete-balanced formulation reducing spurious currents [25]. We compute the interface curvature using second-order height functions defined by PLIC plane position based on the analytical formulation from [26]. Equations (6) and (7) are the projection steps that will ensure mass conservation for the velocity field at the step $(n + 1)$.

3. Simulation setup

The physical domain subject to the simulation is a cube of dimensions L^3 , as shown in Figure 1. The flow is channeled through a tube of length ℓ_x and rectangular cross section with height ℓ_y and width ℓ_z . The bottom plate of the tube ($z = L/2 - \ell_z/2$) is covered with a liquid phase of thickness h , density ρ_l and viscosity μ_l , depicted in the subfigure (c). The gas phase, modeling the exhaled air, has density ρ_a , and viscosity μ_a . It enters the flow from the left wall at $x = 0$ with uniform and constant velocity U through an inflow boundary condition in the tube inner section, $|y - L/2| < \ell_y/2$ and $h - \ell_z/2 < z - L/2 < \ell_z/2$. This condition ensures the inflow of air blows just above the

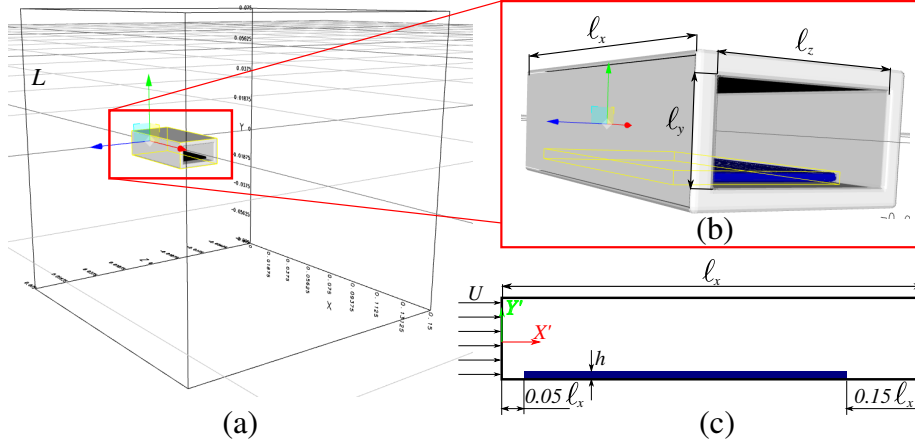


Figure 1: Simulation domain (a), rectangular channel detail (b) and liquid film (c) dimensions.

L	ℓ_x	ℓ_y	ℓ_z	h	ρ_l	μ_l	ρ_a	μ_a	U	σ
0.15	0.05	0.01	0.02	0.001	1000	0.005	1.2	2×10^{-5}	30	0.03

Table 1: Dimensional values of the fluid and geometrical parameters (SI units)

initial position of the liquid layer. The surface tension of the liquid is noted σ . Gravity is neglected as it is small compared to inertial effects $g\ell_z/U^2 \ll 1$.

The main dimensionless parameters are the Reynolds number of the air based on the channel height $Re_a = \rho_a U \ell_y / \mu_a = 18,000$, the Weber number of the air based on the channel height $We_a = \rho_a U^2 \ell_y / \sigma = 360$, and the Reynolds number of the liquid based on the height of the liquid $Re_l = \rho_l U h / \mu_l = 30,000$. The values of these parameters are quite high which makes it surprising that the simulations, performed with a Navier–Stokes code, are still classified as *Direct Numerical Simulations* (DNS).

Indeed the assessment of the DNS character of the simulation may be inferred from the value of the dissipation ϵ in the similar setup of refs. [13, 19]. There the kinetic energy dissipation per unit volume ϵ [27] was measured and it was observed that the maximum value of $\epsilon / (\rho_a U^3 / \ell_z)$ was about 0.01 which yields an estimate of ϵ . The Kolmogorov length scale is then $\eta = (\rho_a \nu_a^3 / \epsilon)^{1/4}$. With the value of ϵ estimated above, we have $\eta_1 \approx 24.2$ microns while the size of the smallest grid cell with the thirteen levels of refinement in the simulation reported here is $\Delta = 2^{-13} L \approx 18.3$ microns. According to the DNS resolution criterion given by Pope [27], the smallest turbulent scales will be well resolved if $\Delta / \eta \leq 2.1$ while we have $\Delta / \eta_1 \approx 0.75$. Even if one uses the more conservative estimate $\eta_2 = \ell_y Re_a^{-3/4}$ as in [20] one gets $\Delta / \eta_2 \approx 2.8$. The perhaps surprising result that the simulations may be qualified as DNS can be explained by the fact that while the less extreme simulations of [13, 19] were limited to $\ell_z / \Delta = 256$ grid points in the gas jet thickness, our simulations using octree refinement

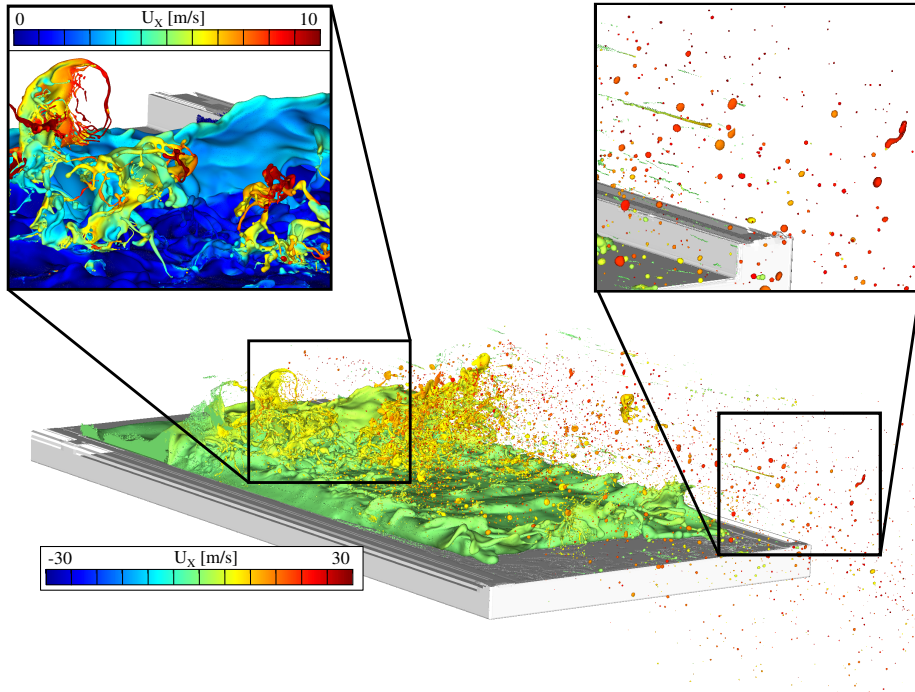


Figure 2: Isometric view of the air-liquid interface at $t=9$ ms. The interface is colored by the U_x velocity component. The droplets by the exit of the tube are close to the stream velocity, as shown in the detail to the right. The left detail employs a different color scale to depict the formation and acceleration of sheets and ligaments in the main wave.

go up to the equivalent of $\ell_z/\Delta = 1092$.

Regarding Adaptive Mesh Refinement (AMR), we use a wavelet-based criterion [28] to limit local f and \vec{u} estimated numerical error. The finest simulation reported employs a maximum refinement level of thirteen (L13), resulting on a grid size of $18.3 \mu\text{m}$. A cartesian grid with this accuracy would have $\approx 5.5 \times 10^{11}$ grid cells while the corresponding octree-grid simulation only scale up to $\approx 3.2 \times 10^9$ cells for the developed spray stage. Simulating 9 ms of physical time take 82 880, 210 446, and 599 040 CPU-hours when using 11, 12 and 13 levels respectively. We run all the simulations at Irene machine (TGCC).

4. Results

Simulations are initialized with zero velocity in the air and liquid although the incompressibility condition results in a non-zero velocity field everywhere in the gas immediately after time zero. The simulation is continued for a total time $T=9$ ms. The liquid surface is quickly significantly perturbed with waves present over the entire length ℓ_x of the tube, with a much larger wave near the inlet and some secondary waves

near the outlet (Figure 2). The wave stretches into a thin liquid layer that fills with air under the combined effect of pressure and vorticity. Eventually, two mechanisms lead to the formation of droplets: the formation of fingers or ligaments at the end of the sheets and the puncturing of the sheets. The latter causes the formation of holes in the sheets and the subsequent expansion of those holes, leading to the formation of ligaments that eventually pinch and break into droplets. This process has been described in other experimental [10] and numerical [13] investigations. In the current “closed channel” configuration similar mechanisms of droplet formation are observed. It is seen on Figure 2 that the small dark red droplets near the channel exit have moved quickly since the drag law scaling for a sphere $F_d \sim \rho_a d^2 U^2 / 4$ (where d is the droplet radius) implies that the small droplets accelerate much faster than the large ones.

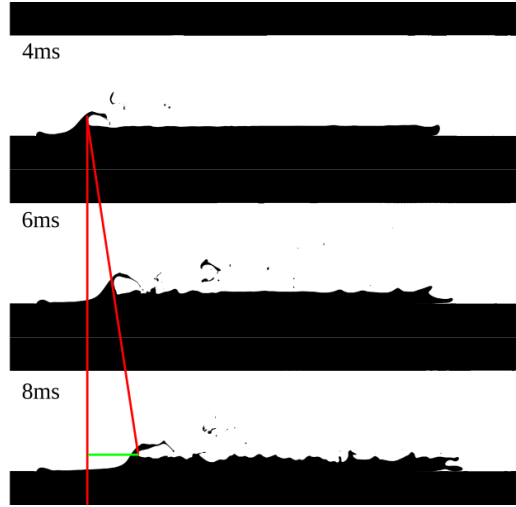


Figure 3: In the middle cross-section of the channel, the liquid phase and the solid are shown in black and the gas phase in white. Three different snapshots at regularly spaced time intervals are shown. The oblique line connects the positions, thus giving a graphical display of the wave velocity U_D , agreeing with the Dimotakis velocity discussed in the text.

A clear phenomenon that couples with droplet formation is growth of a large sheet or wave near the inlet and its progression downstream. The velocity of such waves is typically the Dimotakis velocity [29] and it is expressed as $U_D = U \sqrt{\rho_a} / (\sqrt{\rho_a} + \sqrt{\rho_l})$. A similar kind of solitary wave progressing at the Dimotakis velocity has been observed in the simpler setting of an infinite vortex sheet between air and liquid [30]. The liquid surface is excited by a local perturbation of the flat vortex sheet, and in this case the inhomogeneity of the flow at the entrance plays the role of the localised perturbation, while less localised waves are seen further downstream. In our case the Dimotakis velocity is $U_D \sim 1.004$ m/s which may be compared to a rough measurement from the simulations (Fig. 3) of $U_{D,num} \simeq 1.25$ m/s.

The identification of droplets or connected fluid components, and the computation of their volumes V_d allows to define an equivalent droplet diameter $d = (6V_d/\pi)^{1/3}$.

Figure 4 shows the droplet size distribution for the three simulations performed. We compare only the numerical results, for resolved spherical drops, with the experimental data from Xie *et. al.* [7]; in this article, the Probability Density Function of droplet size is assembled with data from several cough samples, considering a correction for evaporation to better represent the size distribution at the mouth.

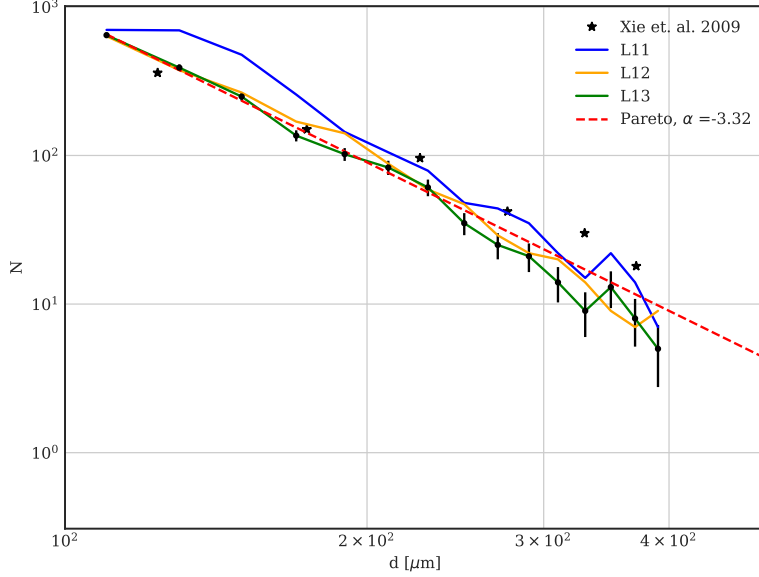


Figure 4: Droplet counts in each bin, proportional to the Probability Distribution Function of droplet diameters from Xie *et. al.* [7] and for the simulations at $t = 9$ ms and for three grid resolutions L13: $\Delta x = 18 \mu\text{m}$, L12: $\Delta x = 36 \mu\text{m}$ and L11: $\Delta x = 72 \mu\text{m}$.

Because of the presence of some non-spherical droplets in the simulation, we filtered the counts, incorporating only near-spherical droplets using a sphericity index. We find that this filtering removes only large droplets, with $d > 200 \mu\text{m}$; there are less than ten of such ligaments. The normalized frequency is shown in Figure 4 together with the statistical error bars, the error being defined as one standard deviation of the binomial. It is seen that the distribution is close to the power law $N(d) \sim d^{-3.32}$ for small sizes and then inches down. On Fig. 4 we do not show droplet counts for $d < 100$ microns and $d > 400$ microns, since the small sizes are plagued by grid resolution errors and the larger sizes by statistical errors. Regarding the comparison with experiments, the simulations predict a smaller amount of large ($d > 200 \mu\text{m}$) drops. Nevertheless, both distributions show an acceptable agreement with the Pareto fit proposed.

5. Discussion

An often considered number frequency (NF) model is the log-normal, which reads $N(d) = (B/d) \exp\left[-(\ln d - \hat{\mu})^2 / (2\hat{\sigma}^2)\right]$ where B is a normalization constant, $\hat{\mu}$ is the ex-

pected value of $\ln d$, also called the *geometric mean*, and σ is the standard deviation of $\ln d$, also called the *geometric standard deviation* (GSD, see [11]). If we plot $y = dP(d)$ versus $x = \ln d$ the Log-Normal frequency distribution appears as a parabola. This is done in Fig. 5. That figure shows a fit with a GSD $\hat{\sigma} = 0.98$. The dimensionless GSD is

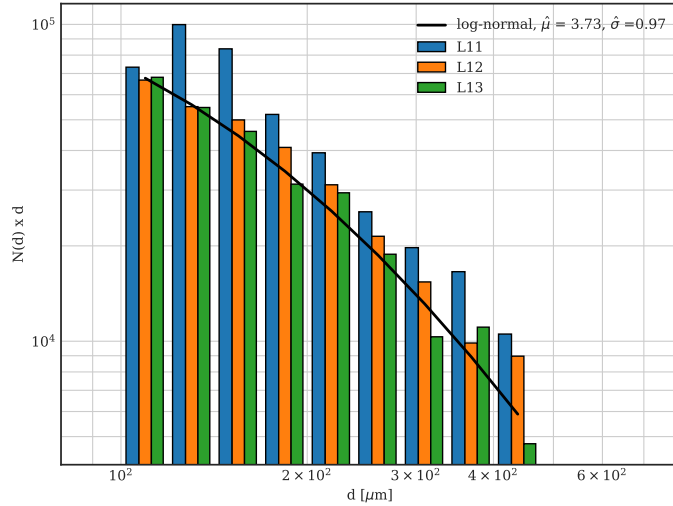


Figure 5: Droplet counts in “log-normal coordinates” in which the log-normal NF appears as a parabola, with labels L11-13 as in Fig. 4.

of the same order of magnitude as the GSD ($\hat{\sigma} \sim 1$) in similar experiments and simulations [31, 13, 32], but in the authors’ opinion, this may not capture universal underlying physics but the similar range of scales that is within numerical or experimental reach in the literature cited. Comparing the NF at various resolution in [31, 13] it is seen that as the grid size is reduced the NF shifts to the left, with its geometric mean decreasing and its GSD increasing. This also seen partially in Fig. 4 where the L11 resolution peaks “before” the two others. It is thus possible that as resolution is increased the curved NF seen on Figs 4 and 5 would progressively asymptote to a power law, that is a Pareto, instead of a converged Log-Normal. Such a Pareto NF necessarily has a lower bound, if only the molecular size. This lower bound is not attainable numerically or perhaps even experimentally. A tempting hypothesis is to associate it to the thickness of the sheets as they break or perforate, which involves mechanisms that are not modelled in this study.

6. Conclusion

We have numerically analyzed a simple physical analog of the physiological mechanism of coughing, based on a previously studied experiment, that is strongly reminiscent of planar sheet atomization processes and presents a reasonable agreement

with experimental data [7]. A Pareto d^{-2} distribution was not found but is not excluded at very small diameters. Perspectives include higher resolutions simulations and laboratory experiments in the regime of this numerical experiment, and using the characteristics of the numerically estimated droplet sizes and velocity to predict the further evolution of the droplet cloud using Lagrangian particle methods such as those of Chong et al. [8].

Acknowledgements

We acknowledge the funding of the CONICET, the Bec.ar programme from the Ministerio de Educación Argentino, the ERC-ADV grant TRUFLOW, the ANR NAN-ODROP grant funded by the *Fondation de France* and the PRACE Covid grant of computer time. We thank Lydia Bourouiba, Pallav Kant, Detlef Lohse and Stéphane Popinet for stimulating and fruitful discussions, and for sharing useful material, visualisations and codes.

References

- [1] L. Bourouiba, E. Dehandschoewercker, J. W. Bush, Violent expiratory events: on coughing and sneezing, *J. Fluid Mech.* 745 (2014) 537–563.
- [2] L. Bourouiba, Turbulent gas clouds and respiratory pathogen emissions: potential implications for reducing transmission of covid-19, *JAMA* 323 (18) (2020) 1837–1838.
- [3] S. Balachandar, S. Zaleski, A. Soldati, G. Ahmadi, L. Bourouiba, Host-to-host airborne transmission as a multiphase flow problem for science-based social distance guidelines, *International Journal of Multiphase Flow* 132 (2020) 103439.
- [4] L. Bourouiba, The fluid dynamics of disease transmission, *Annual Review of Fluid Mechanics* 53 (2020).
- [5] J. P. Duguid, The size and the duration of air-carriage of respiratory droplets and droplet-nuclei, *Epidemiology & Infection* 44 (6) (1946) 471–479.
- [6] R. Loudon, R. Roberts, Relation between the airborne diameters of respiratory droplets and the diameter of the stains left after recovery, *Nature* 213 (5071) (1967) 95–96.
- [7] X. Xie, Y. Li, H. Sun, L. Liu, Exhaled droplets due to talking and coughing, *Journal of the Royal Society Interface* 6 (suppl.6) (2009) S703–S714.
- [8] K. L. Chong, C. S. Ng, N. Hori, R. Yang, R. Verzicco, D. Lohse, Extended lifetime of respiratory droplets in a turbulent vapour puff and its implications on airborne disease transmission, arXiv preprint arXiv:2008.01841 (2020).
- [9] T. Dbouk, D. Drikakis, On coughing and airborne droplet transmission to humans, *Physics of Fluids* 32 (5) (2020) 053310.

- [10] B. Scharfman, A. Techet, J. Bush, L. Bourouiba, Visualization of sneeze ejecta: steps of fluid fragmentation leading to respiratory droplets, *Experiments in Fluids* 57 (2) (2016) 24.
- [11] M. Nicas, W. W. Nazaroff, A. Hubbard, Toward Understanding the Risk of Secondary Airborne Infection: Emission of Respirable Pathogens, *Journal of Occupational and Environmental Hygiene* 2 (3) (2017) 143–154.
- [12] W. F. Wells, et al., *Airborne Contagion and Air Hygiene. An Ecological Study of Droplet Infections.*, Cambridge: Harvard University Press (for The Commonwealth Fund), Mass., USA., 1955.
- [13] Y. Ling, D. Fuster, S. Zaleski, G. Tryggvason, Spray formation in a quasiplanar gas–liquid mixing layer at moderate density ratios: A numerical closeup, *Phys. Rev. Fluids* 2 (1) (2017) 014005.
- [14] E. Villermaux, B. Bossa, Drop fragmentation on impact, *J. Fluid Mech.* 668 (2011) 412–435.
- [15] M. King, G. Brock, C. Lundell, Clearance of mucus by simulated cough, *physiology.org* 58 (6) (1985) 1776–1782.
- [16] M. Gorokhovski, M. Herrmann, Modeling primary atomization, *Annu. Rev. Fluid Mech.* 40 (2008) 343–366.
- [17] G. Agbaglah, R. Chiodi, O. Desjardins, Numerical simulation of the initial destabilization of an air-blasted liquid layer, *J. Fluid Mech.* 812 (2017) 1024–1038.
- [18] A. Zandian, W. A. Sirignano, F. Hussain, Length-scale cascade and spread rate of atomizing planar liquid jets, *International Journal of Multiphase Flow* 113 (2019) 117–141.
- [19] Y. Ling, D. Fuster, G. Tryggvason, S. Zaleski, A two-phase mixing layer between parallel gas and liquid streams: multiphase turbulence statistics and influence of interfacial instability, *J. Fluid Mech.* 859 (2019) 268–307.
- [20] C. R. Constante-Amores, L. Kahouadji, A. Batchvarov, S. Shin, J. Chergui, D. Juric, O. K. Matar, Direct numerical simulations of transient turbulent jets: vortex-interface interactions, *arXiv preprint arXiv:2012.01887* (2020).
- [21] G. Tryggvason, R. Scardovelli, S. Zaleski, *Direct Numerical Simulations of Gas-Liquid Multiphase Flows*, Cambridge University Press, 2011.
- [22] S. Popinet, An accurate adaptive solver for surface-tension-driven interfacial flows, *J. Comput. Phys.* 228 (16) (2009) 5838–5866.
- [23] G. D. Weymouth, D. K.-P. Yue, Conservative volume-of-fluid method for free-surface simulations on cartesian-grids, *Journal of Computational Physics* 229 (8) (2010) 2853–2865.

- [24] C. I. Pairetti, S. M. Damián, N. M. Nigro, S. Popinet, S. Zaleski, Mesh resolution effects on primary atomization simulations, *Atomization and Sprays* 30 (12) (2020).
- [25] S. Popinet, Numerical models of surface tension, *Annual Review of Fluid Mechanics* 50 (2018) 49–75.
- [26] R. Scardovelli, S. Zaleski, Direct numerical simulation of free-surface and interfacial flow, *Annual review of fluid mechanics* 31 (1) (1999) 567–603.
- [27] S. B. Pope, *Turbulent flows* (2001).
- [28] J. A. van Hooft, S. Popinet, C. C. van Heerwaarden, S. J. van der Linden, S. R. de Roode, B. J. van de Wiel, Towards adaptive grids for atmospheric boundary-layer simulations, *Boundary-Layer Meteorology* (2018) 1–23.
- [29] P. Dimotakis, Entrainment and growth of a fully developed, two-dimensional shear layer, *AIAA J* 24 (1986) 1791–1796.
- [30] J. Hoepffner, R. Blumenthal, S. Zaleski, Self-similar wave produced by local perturbation of the Kelvin-Helmholtz shear-layer instability, *Phys. Rev. Lett* 106 (2011) 104502.
- [31] M. Herrmann, On Simulating Primary Atomization Using the Refined Level Set Grid Method, *AAS* 21 (4) (2011) 283–301.
- [32] S. Marty, Contribution à l’étude de l’atomisation assistée d’un liquide : instabilité de cisaillement et génération du spray, Ph.D. thesis, Université Grenoble Alpes, Université de Grenoble (Apr. 2015).